


Synthetic Topological Vacua of Yang-Mills Fields in Bose-Einstein Condensates

Jia-Zhen Li,^{1,*} Cong-Jun Zou,^{1,*} Yan-Xiong Du,¹ Qing-Xian Lv,¹ Wei Huang,¹ Zhen-Tao Liang,¹ Dan-Wei Zhang,^{1,2}
 Hui Yan,^{1,2,3} Shanchao Zhang^{1,2,†} and Shi-Liang Zhu^{1,2,‡}

¹Guangdong Provincial Key Laboratory of Quantum Engineering and Quantum Materials,
 School of Physics and Telecommunication Engineering, South China Normal University,
 Guangzhou 510006, China

²Guangdong-Hong Kong Joint Laboratory of Quantum Matter, Frontier Research Institute for Physics,
 South China Normal University, Guangzhou 510006, China

³Guangdong Provincial Engineering Technology Research Center for Quantum Precision Measurement,
 South China Normal University, Guangzhou 510006, China

 (Received 16 July 2022; revised 24 September 2022; accepted 1 November 2022; published 22 November 2022)

Topological vacua are a family of degenerate ground states of Yang-Mills fields with zero field strength but nontrivial topological structures. They play a fundamental role in particle physics and quantum field theory, but have not yet been experimentally observed. Here we report the first theoretical proposal and experimental realization of synthetic topological vacua with a cloud of atomic Bose-Einstein condensates. Our setup provides a promising platform to demonstrate the fundamental concept that a vacuum, rather than being empty, has rich spatial structures. The Hamiltonian for the vacuum of topological number $n = 1$ is synthesized and the related Hopf index is measured. The vacuum of topological number $n = 2$ is also realized, and we find that vacua with different topological numbers have distinctive spin textures and Hopf links. Our Letter opens up opportunities for exploring topological vacua and related long-sought-after instantons in tabletop experiments.

DOI: [10.1103/PhysRevLett.129.220402](https://doi.org/10.1103/PhysRevLett.129.220402)

Introduction.—The vacuum of a gauge field is the field state with the lowest energy and thus zero field strength. It is crucial to our understanding of some amazing features of particle structures and quantum fields [1,2]. For example, in quantum electrodynamics, a familiar vacuum is the zero-point fluctuation of the electromagnetic field, which leads to important physical effects such as the Lamb shift, anomalous magnetic moment of electrons, and Casimir force. As another example, in the electroweak theory, the investigation of vacuum leads to our deep understanding of the spontaneous symmetry breaking of vacuum, the origin of mass, and the predication of the Higgs bosons. Furthermore, the studies of the quantum chromodynamics vacuum may explain the origin and value of the quark and gluon condensates, the mechanism for quark confinement and chiral symmetry breaking [1,2].

The non-Abelian Yang-Mills field is predicted to have an intriguing type of topological vacua (TV), namely, a family of degenerate ground states with zero field strength but nontrivial topological structures [2–5]. This type of vacua is predicted to be significantly different from an Abelian vacuum in terms of energy degeneracy and field topology. Furthermore, quasiparticles called instantons are known to describe tunneling processes between different vacua, which lead to the introduction of the CP -violating θ term and shed light on the mechanism of quark confinement [1,2]. These nonperturbative solutions of the Yang-Mills

fields were first proposed in 1975 [3], but have not yet been experimentally observed.

Inspired by the realization of the Abelian Higgs model with Bose-Einstein condensates (BECs) [6,7] and the rapidly developing quantum simulation of synthetic gauge fields in ultracold atoms [8–18] and other quantum-engineered systems [19,20], in this Letter, we theoretically propose and experimentally realize the first scheme to synthesize TV of Yang-Mills fields using a cloud of ultracold atomic BECs coupled with a pair of Raman laser fields. The exemplary TV with topological number (TN) $n = 1$ is realized and the related Hopf index is measured. Furthermore, both the three-dimensional spin textures and Hopf links of this family of TV with $n = 1$ and 2 are demonstrated. Our Letter opens up a potential way to study TV with engineered quantum systems.

Topological vacua of the Yang-Mills fields.—A gauge field is fully described by a gauge potential A_μ . The commonly studied kinetic effects of a field are determined by the field strength $F_{\mu\nu} \equiv \partial_\mu A_\nu - \partial_\nu A_\mu - i[A_\mu, A_\nu]$. Notably, a gauge field also has geometric effects, such as the Aharonov-Bohm effect, which are solely determined by A_μ . It is worth noting that for the same $F_{\mu\nu}$, there exist a group of gauge potentials A_μ 's that are connected by gauge transformations described by $N \times N$ unitary matrices $U(N)$. With an Abelian vacuum, $F_{\mu\nu} = 0$ results in the only choice of $A_\mu = 0$. However, for a non-Abelian $U(N)$,

besides the regular vacuum with $A_\mu = 0$, there are a group of $A_\mu = U^{-1}\partial_\mu U$ gauge potentials that possess rich geometric effects. Searching for nonperturbative solutions of the $SU(2)$ Yang-Mills fields reveals a family of solutions described by the gauge transformations $U_n = (U_1)^n$ with n being an integer [3–5], where

$$U_1(\mathbf{r}) = \frac{r^2 - \eta^2}{r^2 + \eta^2} \sigma_0 - \frac{2i\eta \mathbf{r} \cdot \vec{\sigma}}{r^2 + \eta^2}. \quad (1)$$

Here $\vec{\sigma} = (\sigma_x, \sigma_y, \sigma_z)$ are Pauli matrices, σ_0 is the identity matrix, $\mathbf{r} = (x, y, z)$ is the position vector with $r = |\mathbf{r}|$, and η is a constant. As can be seen, the field strength $F_{\mu\nu}$ related to gauge transformation $U_n = (U_1)^n$ vanishes and thus they represent degenerate vacua. Interestingly, these vacua are characterized by a TN,

$$n = \frac{1}{24\pi^2} \int_{-\infty}^{+\infty} d\mathbf{r} \epsilon_{ijk} \text{Tr}(U_n^{-1} \partial_i U_n U_n^{-1} \partial_j U_n U_n^{-1} \partial_k U_n), \quad (2)$$

where ϵ_{ijk} is the Levi-Civita symbol. As shown in Fig. 1(a), there must exist potential barriers to separate vacua with

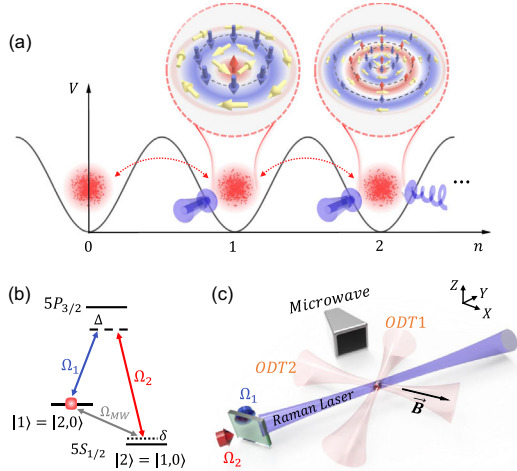


FIG. 1. Scheme of a family of TV synthesized with ultracold atoms and experimental realization. (a) Schematic plot of the potential energy $V[\mathbf{A}]$ as a function of the TN n . The vacuum with fixed TN has specific spin textures. Quantum tunneling between vacua is allowed with the assistance of instantons. (b) Proposed atomic energy level configuration. Two Zeeman sublevels that belong to the ground hyperfine manifolds of ^{87}Rb atoms are selected: $|1\rangle = |5^1S_{1/2}, F=2, m_F=0\rangle$ and $|2\rangle = |5^1S_{1/2}, F=1, m_F=0\rangle$, which are cyclically coupled via a detuned two-photon Raman process ($\Omega_{1,2}$) together with a microwave (Ω_{MW}). (c) Experiment setup. A cloud of ^{87}Rb BEC are trapped in a crossed optical dipole trap (ODT). A homogeneous magnetic field along the x axis sets the quantum axis. A pair of copropagating Raman lasers $\Omega_{1,2}$ focused at the cloud couple the two states $|1\rangle$ and $|2\rangle$. A microwave field emitted from a microwave waveguide is used to realize the initial state preparation and synthesized vacua measurement.

different TNs. Accompanied by instantons, quantum transition between vacua is predicted [1,2,4].

Artificial gauge fields for a light-atom system.—Here we use atomic BECs to demonstrate that TV can be synthesized with an engineered quantum system. The Hamiltonian of a laser-atom interaction system reads $H = (\mathbf{p}^2/2m) + V(\mathbf{r}) + H_{\text{AL}}$, where m is the atomic mass, the laser-atom interaction H_{AL} is an $N \times N$ matrix in the basis of the internal energy levels $|j\rangle$, and the potential $V(\mathbf{r}) = \sum_{j=1}^N V_j(\mathbf{r})|j\rangle\langle j|$. In this case, the full quantum state can be expanded as $|\Phi(\mathbf{r})\rangle = \sum_{j=1}^N \phi_j(\mathbf{r})|j\rangle$.

In the representation of the dressed states $|\chi_n\rangle$ that are eigenvectors of the Hamiltonian H_{AL} , $H_{\text{AL}}|\chi_n\rangle = \epsilon_n|\chi_n\rangle$, the full quantum state of the atom $|\tilde{\Phi}(\mathbf{r})\rangle$ is written as $|\tilde{\Phi}(\mathbf{r})\rangle = \sum_j \psi_j(\mathbf{r})|\chi_j(\mathbf{r})\rangle$, where the wave functions $|\tilde{\Psi}\rangle = (|\psi_1\rangle, |\psi_2\rangle, \dots, |\psi_N\rangle)^\top$ obey the Schrödinger equation $i\hbar(\partial/\partial t)|\tilde{\Psi}\rangle = \tilde{H}_{\text{eff}}|\tilde{\Psi}\rangle$, with the effective Hamiltonian $\tilde{H}_{\text{eff}} = UH_{\text{eff}}U^\dagger$. We further assume that the first 2 atomic dressed states among the total N states are degenerate and are well separated from the remaining $N-2$ states. This way, we can project the full Hamiltonian onto this subspace. Under this condition, the wave function in the subspace $\Psi = (\psi_1, \psi_2)^\top$ is again governed by the Schrödinger equation $i\hbar(\partial/\partial t)\Psi = H_{\text{eff}}\Psi$ with the effective Hamiltonian taking the following form [21–25]:

$$H_{\text{eff}} = \frac{1}{2m}(-i\hbar\nabla - \mathbf{A})^2 + V_{\text{eff}}. \quad (3)$$

Here $\mathbf{A} = i\hbar U\nabla U^\dagger$ with $U = (|\chi_1\rangle, |\chi_2\rangle)$ and V_{eff} is a scalar potential in Supplemental Material (SM) [26].

Realizing topological vacua with atoms.—Topological vacua can be realized using ultracold atoms with two fully (or almost) degenerate states by designing the laser-atom interactions. Two degenerate states can be achieved with four-level atoms, such as a tripod-level or ∞ -level configuration [16,18]. For experimental simplicity, we propose a feasible scheme with two almost degenerate states. We consider three-level atoms cyclically coupled by three position-dependent fields $\Omega_{1,2}(\mathbf{r})$ and $\Omega_{\text{MW}}(\mathbf{r})$, as shown in Fig. 1(b). The Hamiltonian $H_{\text{AL}}(\mathbf{r})$ can be written as

$$H_{\text{AL}}(\mathbf{r}) = \frac{\hbar}{2} \begin{pmatrix} 0 & \Omega_{\text{MW}}^*(\mathbf{r}) & \Omega_1^*(\mathbf{r}) \\ \Omega_{\text{MW}}(\mathbf{r}) & -2\alpha(\mathbf{r})|\delta(\mathbf{r})| & \Omega_2^*(\mathbf{r}) \\ \Omega_1(\mathbf{r}) & \Omega_2(\mathbf{r}) & 2\alpha(\mathbf{r})|\Delta(\mathbf{r})| \end{pmatrix}, \quad (4)$$

where $\Delta(\mathbf{r})$ [$\delta(\mathbf{r})$] is the single-photon [two-photon] detuning and $\alpha(\mathbf{r}) = \text{sgn}(|\mathbf{r}| - 1)$ is a sign function.

In order to easily obtain a solution for the TV, we assume $\Omega_{\text{MW}}(\mathbf{r}) = -i\Omega_1(\mathbf{r})\sqrt{|\delta(\mathbf{r})/\Delta(\mathbf{r})|}$. To simplify the notations, we hide the notation \mathbf{r} later on. We solve the Schrödinger equation $H_{\text{AL}}|\chi_n\rangle = \epsilon_n|\chi_n\rangle$ under the large detuning

condition, i.e., $\Delta \gg |\delta|, \Omega$, with $\Omega = \sqrt{|\Omega_1|^2 + |\Omega_2|^2}$, and then obtain the eigenvalues $\varepsilon \approx 0, -\hbar\kappa^2/(4\Delta), \hbar[\Delta + \Omega^2/(4\Delta)]$ with $\kappa = \sqrt{\Omega^2 + 4|\delta\Delta|}$. The first two are nearly degenerate since there is a large gap between the first two and the last one. They may create a subspace for synthetic SU(2) gauge field. To clearly present that $\{|\chi_1\rangle, |\chi_2\rangle\}$ form a pseudospin subspace, we denote them as $\{|\chi_-\rangle, |\chi_+\rangle\}$. After solving the related eigenvectors, we derive the transformation

$$U_{\text{AL}} = \frac{1}{\kappa} \begin{pmatrix} -i\Omega_2 + 2\alpha\sqrt{|\delta\Delta|} & i\Omega_1^* \\ i\Omega_1 & i\Omega_2 + 2\alpha\sqrt{|\delta\Delta|} \end{pmatrix}. \quad (5)$$

Therefore, if we can find a solution with $U_{\text{AL}} = U_n$, then a TV with TN n is realizable. In SM [26], we show such solutions. In particular, we find that $\Omega = 2\sqrt{|\delta\Delta|} \times \tan[2\arctan(r/\eta)]$ leads to $U_{\text{AL}} = U_1$. We can further realize vacua with different TN n in an array configuration as shown in Fig. 1(a), and then instantons can emerge in such an array [27].

We can realize the SU(2) Yang-Mills vacua with desired $U_n(\mathbf{r})$ if we implement the laser-atom interaction to obtain the topologically equivalent Hamiltonian $H_{\text{TV}}(\mathbf{r}) = U_n(\mathbf{r})\sigma_z U_n^\dagger(\mathbf{r})$. However, engineering such a Hamiltonian in real space is challenging since the strength, frequency, and phase of the coupling fields in each spatial point must be well designed. In the first experiment, we simply implement the above $H_{\text{TV}}(\mathbf{r})$ in a parameter space and then measure the TN and the related significant properties of the TV. Our experiment can visualize the spatial structure of the TV, which has not been explored in previous literature.

The TN in Eq. (2) is equivalent to the Hopf index χ_{Hopf} [22,26,28,29],

$$n = \chi_{\text{Hopf}} = -\frac{1}{4\pi^2} \int_{-\infty}^{+\infty} d\mathbf{r} \mathbf{a}(\mathbf{r}) \cdot \mathbf{f}(\mathbf{r}), \quad (6)$$

where the k th component of $\mathbf{a}(\mathbf{r})$ defined as $\mathbf{a}_k(\mathbf{r}) = \langle \chi_-(\mathbf{r}) | \partial_k | \chi_-(\mathbf{r}) \rangle$ is Berry connection and $\mathbf{f}(\mathbf{r}) = \nabla \times \mathbf{a}(\mathbf{r})$ is Berry curvature [21]. Experimentally, we can obtain both $\mathbf{a}(\mathbf{r})$ and $\mathbf{f}(\mathbf{r})$ by adiabatically tuning the Raman laser fields and detecting the state $|\chi_-(\mathbf{r})\rangle$. According to Eq. (6), the TN can be measured by detecting the spin states of the atoms in the full space of \mathbf{r} . Furthermore, the properties of the vacuum can be determined by the density matrices $\langle \sigma \rangle = \{ \langle \chi_- | \sigma_x | \chi_- \rangle, \langle \chi_- | \sigma_y | \chi_- \rangle, \langle \chi_- | \sigma_z | \chi_- \rangle \}$ [26].

Experimental scheme.—The schematics of our experiment setup is shown in Fig. 1. A cloud of ^{87}Rb atoms are laser cooled in a magneto-optical trap and then evaporatively cooled down to BEC state in a far off-resonant crossed optical dipole trap (ODT). A weak homogeneous magnetic field \mathbf{B} along the x axis sets a quantum axis. In order to maintain a long coherence time, we choose two quantum states $|1\rangle$ and $|2\rangle$ from the magnetic insensitive hyperfine Zeeman sublevels to mimic the pseudospin.

Initially, all atoms are polarized in pseudospin state $|1\rangle$ by a coherent microwave pulse.

The expected Hamiltonian $H_{\text{TV}}(\mathbf{r})$ at specified position \mathbf{r} is realized by adding two Raman lasers with respective Rabi frequency Ω_1 and Ω_2 . As shown in the energy level configuration in Fig. 1(b), the paired Raman lasers couple the two spin states $|1\rangle$ and $|2\rangle$ via two-photon process. The effects of excited states are adiabatically eliminated by setting $\Delta = 2\pi \times 3.9$ THz since both $\Omega_{1,2}$ and δ are on the order of $2\pi \times 10$ kHz. The third coupling field Ω_{MW} is estimated to be around 1 Hz and hence can be safely omitted. Therefore, the two quantum states $|1\rangle$ and $|2\rangle$, together with the paired Raman lasers, produce an approximate degenerate sub-Hilbert space.

To detect the state $|\chi_-\rangle$ at each position \mathbf{r} , we manipulate the Hamiltonian H_{TV} adiabatically and drive the atoms from the initial state $|1\rangle$ to the final state $|\chi_-\rangle$ in an adiabatic way. In our experiment, the largest Rabi frequency Ω_M is $2\pi \times 28.5$ kHz, while the coherence time of spin states is longer than 8 ms. For adiabatic state evolution, the single photon detuning Δ is kept almost constant while the Raman coupling strength Ω_R and two-photon detuning δ ramp smoothly from the respective initial value of $\Omega_R = 0$ and $\delta = \Omega_M$. The whole evolution time is set to around $350 \mu\text{s}$ ($\sim 20\pi/\Omega_M$), which is longer compared to the typical time of Rabi oscillation but much shorter than the coherence time and thus ensures the adiabatic and coherent state evolution. With this method, we may adiabatically prepare one Hamiltonian $H_{\text{TV}}(\mathbf{r})$ at arbitrary parameter \mathbf{r} in a single experiment run, during which atoms are loaded into the expected state $|\chi_-\rangle$ and ready for detections.

Measuring the topological number.—We first synthesize the TV of $n = 1$. Along all three x, y, z directions, we take the step size 0.1 and range of \mathbf{r} as $-3 \leq x, y, z \leq 3$. Here and in the following, the nonzero parameter η in Eq. (1) is taken as the length unit of x, y, z [30]. To detect TN, we achieve the Berry curvature $\mathbf{f}(\mathbf{r})$ point by point by measuring the density matrix of atoms at each point in the parameter space. Because of the gauge choice problem, it is difficult to directly measure the Berry connection $\mathbf{a}(\mathbf{r})$. As long as a specified gauge is chosen, the Berry connection at each point could be derived from the measured distribution of Berry curvature $\mathbf{f}(\mathbf{r})$. Eventually, the TN can be obtained by summing up the inner product of $\mathbf{f}(\mathbf{r})$ and $\mathbf{a}(\mathbf{r})$ at all the measured points [26]. By repeating the Hamiltonian H_{TV} preparation and spin density matrix measurement at each point of \mathbf{r} , we measure the Hopf index of U_1 as $n = 0.91$, which is limited by the average Hamiltonian preparation fidelity of 0.97 ± 0.03 . The fidelity is evaluated according to the measured density matrices at all points, and the error is standard deviation.

Spin texture.—Intriguingly, our setup provides a unique platform to demonstrate that vacua have rich spatial structures. We reveal that the distribution of $U(\mathbf{r})$ can be used to visualize the topological structure of a vacuum and

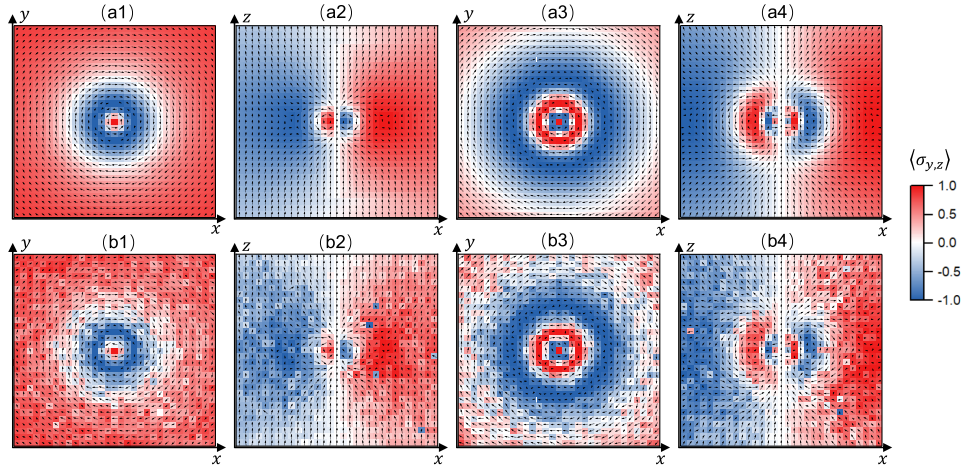


FIG. 2. The topologies of vacua visualized by spatial distribution of atomic spin direction. (a1)–(a4) Theoretical results of density matrices that show the direction of atomic pseudospin. (b1)–(b4) Experimentally measured results. Panels (a1) and (b1) correspond to the spin texture of the vacuum with $n = 1$ in the plane of $z = 0$, while panels (a2) and (b2) are those in the plane of $y = 0$. Panels (a3) and (b3) correspond to the spin texture of the vacuum with $n = 2$ in the plane of $z = 0$, while panels (a4) and (b4) are those in the plane of $y = 0$. Black arrows represent the in-plane components, while colors (with values mapped to the right-hand-side color bar) indicate the remaining components perpendicular to the plane.

that the vacua with different TNs have distinctive spatial spin textures. As $U(\mathbf{r}) = (|\chi_+(\mathbf{r})\rangle, |\chi_-(\mathbf{r})\rangle)$ in our experiment and $|\chi_+(\mathbf{r})\rangle, |\chi_-(\mathbf{r})\rangle$ are always orthogonal to each other, the spin state $|\chi_-(\mathbf{r})\rangle$ can well demonstrate the properties of the synthesized vacuum. In order to show these structures, we utilize $\langle \sigma \rangle$ to depict the spatial textures of atomic spins.

Spin texture in the horizontal xy plane of $z = 0$ and vertical yz plane of $x = 0$ are measured. The measurements are conducted at each point with grid spacing 0.3 and the range $-5 \leq x, y, z \leq 5$. The spin textures of the vacua with $n = 1$ and $n = 2$ are plotted in Figs. 2(a1)–2(a4). As an example, Fig. 2(a1) shows spin textures in the xy plane with $z = 0$. The black arrows indicate the direction of the in-plane xy components $\langle \sigma_x \rangle$ and $\langle \sigma_y \rangle$, while colors depict the magnitude of z component $\langle \sigma_z \rangle$.

The topologies of the vacua can be intuitively understood by checking the rotation of the spin texture. For $n = 1$, as shown in Figs. 2(a1) and 2(b1), all directions of $\langle \sigma_x \rangle, \langle \sigma_y \rangle$, and $\langle \sigma_z \rangle$ reverse one time in space, which means that the spin texture reverses its direction once from the center of the space to the outside. At both the center and the infinity far away region in Figs. 2(a1) and 2(b1), all spins point to the positive z axis with $\langle \sigma_z \rangle = 1$. In between, there exists a (deep blue) ring shape where all spins point to the negative z axis with $\langle \sigma_z \rangle = -1$. This spin texture suggests that the gauge potential twists one time in space, which can be more clearly seen in the vertical yz plane with $x = 0$ from the arrow direction shown in Figs. 2(a2) and 2(b2).

Spin textures have significant differences between vacua $n = 1$ and $n = 2$, as shown in Figs. 2(a3) and 2(b3) and in Figs. 2(a4) and 2(b4). In both cases, the spins point to the positive z axis both at the center and the infinity far away

region, but there are two ring shapes for vacuum $n = 2$ where all spins point to the negative z axis. Therefore, the spins twist twice in space for the $n = 2$ vacuum [31].

Hopf links.—We further show that Hopf links are another powerful way to reveal the intrinsic spatial structure of the TV. A Hopf link is a trace of points where the spin points to the same direction. It has been used to investigate topological solitons [22,32,33] and the topological properties in the

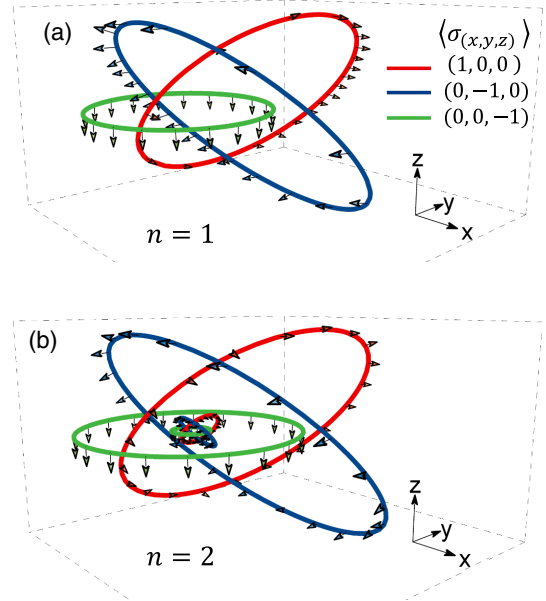


FIG. 3. Hopf links of topological vacua. Hopf links with (a) $n = 1$ and (b) $n = 2$. Hopf links belonging to spin directions in the positive x , negative y , and negative z axis are plotted in red, blue, and green, respectively. Solid lines are theoretical results, and arrows denote the spin direction determined by the measured data.

Brillouin zone (a three-torus T^3) [29,34]. The link space here is an ordinary infinite space \mathcal{R}^3 . To understand the vacuum structures, we plot exemplary Hopf links for $n = 1$ and $n = 2$ in the three-dimensional parameter space, as shown in Fig. 3. We select three typical directions (positive x axis, negative y axis, and z axis) to plot Hopf links, which are theoretically depicted by the solid red, blue, and green lines, respectively. The spin texture at a series of points on each line are experimentally measured and shown by arrows in Fig. 3. For the $n = 1$ vacuum, there is only one link for each spin direction and these three Hopf links interwind with each other one time in space. When the TN of the vacuum is $n = 2$, there exist two separate links for each spin direction. The 6 total links are in 2 different groups; in each group, the links of different spin directions interwind with each other one time. Therefore, the total TNs are equally contributed by the two groups of spin winding.

Conclusion.—In summary, we have reported the first experiment to realize synthetic TV and explored their nontrivial properties. These results establish the first experimental platform to explore the fundamental structure of TV. Our Letter can be extended to other quantum-engineered systems, such as superconducting qubits and trapped ions. Our theoretical scheme can be applied to realizing a three-dimensional real space TV and an array of TV as shown in Fig. 1(a) and in Fig. S1 in SM [26]. Although such experiments are challenging, once they are realized, the long-sought-after instantons and nonperturbative features of the Yang-Mills fields can be explored in tabletop experiments. However, just as many work on this direction [8–20], our simulated SU(2) gauge field is a kind of fixed classical gauge field felt by particles and it does not have its own dynamics. Combined with the recently developed technologies of creating synthetic gauge fields with its own dynamics [35], our Letter may shed light on simulating the vacua of the quantized Yang-Mills fields, which is an open question in quantum field theory.

We thank Y. Q. Zhu for his contributions on the detection of the Hopf index, and D. L. Deng, L. M. Duan, and Y. X. Zhao for helpful discussions. This work was supported by the Key-Area Research and Development Program of Guangdong Province (Grant No. 2019B030330001), the National Key Research and Development Program of China (Grant No. 2020YFA0309500), and the National Natural Science Foundation of China (Grants No. U20A2074, No. 12074132, No. 12074180, No. 12174126, No. 12104168, and No. U1801661).

*These authors contributed equally to this work.

†sczhang@m.scnu.edu.cn

*slzhu@scnu.edu.cn

[1] S. Weinberg, *The Quantum Theory of Fields* (Cambridge University Press, Cambridge, England, 1996).

- [2] E. Bick and F.D. Steffen, *Topology and Geometry in Physics* (Springer-Verlag, Berlin, 2005).
- [3] A. Belavin, A. Polyakov, A. Schwartz, and Y. Tyupkin, Pseudoparticle solutions of the Yang-Mills equations, *Phys. Lett.* **59B**, 85 (1975).
- [4] G. 't Hooft, Symmetry Breaking through Bell-Jackiw Anomalies, *Phys. Rev. Lett.* **37**, 8 (1976).
- [5] R. Jackiw and C. Rebbi, Vacuum Periodicity in a Yang-Mills Quantum Theory, *Phys. Rev. Lett.* **37**, 172 (1976).
- [6] J. Leonard, A. Morales, P. Zupancic, T. Donner, and T. Esslinger, Monitoring and manipulating Higgs and Goldstone modes in a supersolid quantum gas, *Science* **358**, 1415 (2017).
- [7] Manuel Endres, Takeshi Fukuhara, David Pekker, Marc Cheneau, Peter Schauß, Christian Gross, Eugene Demler, Stefan Kuhr, and Immanuel Bloch, The Higgs amplitude mode at the two-dimensional superfluid/Mott insulator transition, *Nature (London)* **487**, 454 (2012).
- [8] Y.J. Lin, R. L. Compton, A. R. Perry, W. D. Phillips, J. V. Porto, and I. B. Spielman, Bose-Einstein Condensate in a Uniform Light-Induced Vector Potential, *Phys. Rev. Lett.* **102**, 130401 (2009).
- [9] M. C. Beeler, R. A. Williams, K. Jiménez-García, L. J. LeBlanc, A. R. Perry, and I. B. Spielman, The spin Hall effect in a quantum gas, *Nature (London)* **498**, 201 (2013).
- [10] L. Duca, T. Li, M. Reitter, I. Bloch, M. Schleier-Smith, and U. Schneider, An Aharonov-Bohm interferometer for determining Bloch band topology, *Science* **347**, 288 (2015).
- [11] Zhan Wu, Long Zhang, Wei Sun, Xiao-Tian Xu, Bao-Zong Wang, Si-Cong Ji, Youjin Deng, Shuai Chen, Xiong-Jun Liu, and Jian-Wei Pan, Realization of two-dimensional spin-orbit coupling for Bose-Einstein condensates, *Science* **354**, 83 (2016).
- [12] Lianghai Huang, Zengming Meng, Pengjun Wang, Peng Peng, Shao-Liang Zhang, Liangchao Chen, Donghao Li, Qi Zhou, and Jing Zhang, Experimental realization of two-dimensional synthetic spin-orbit coupling in ultracold Fermi gases, *Nat. Phys.* **12**, 540 (2016).
- [13] S. Kolkowitz, S. L. Bromley, T. Bothwell, M. L. Wall, G. E. Marti, A. P. Koller, X. Zhang, A. M. Rey, and J. Ye, Spin-orbit-coupled fermions in an optical lattice clock, *Nature (London)* **542**, 66 (2017).
- [14] S. Sugawa, F. Salces-Carcoba, A. R. Perry, Y. Yue, and I. B. Spielman, Second Chern number of a quantum-simulated non-Abelian Yang monopole, *Science* **360**, 1429 (2018).
- [15] Richard J. Fletcher, Airlia Shaffer, Cedric C. Wilson, Parth B. Patel, Zhenjie Yan, Valentin Crépel, Biswaroop Mukherjee, and Martin W. Zwierlein, Geometric squeezing into the lowest Landau level, *Science* **372**, 1318 (2021).
- [16] Q. X. Lv *et al.*, Measurement of Spin Chern Numbers in Quantum Simulated Topological Insulators, *Phys. Rev. Lett.* **127**, 136802 (2021).
- [17] J. Dalibard, F. Gerbier, G. Juzeliūnas, and P. Ohberg, Artificial gauge potentials for neutral atoms, *Rev. Mod. Phys.* **83**, 1523 (2011).
- [18] D. W. Zhang, Y. Q. Zhu, Y. X. Zhao, H. Yan, and S. L. Zhu, Topological quantum matter with cold atoms, *Adv. Phys.* **67**, 253 (2018).

- [19] X. Tan *et al.*, Experimental Observation of Tensor Monopoles with a Superconducting Qudit, *Phys. Rev. Lett.* **126**, 017702 (2021).
- [20] Mo Chen, Changhao Li, Giandomenico Palumbo, Yan-Qing Zhu, Nathan Goldman, and Paola Cappellaro, A synthetic monopole source of Kalb-Ramond field in diamond, *Science* **375**, 1017 (2022).
- [21] M. V. Berry, Quantal phase factors accompanying adiabatic changes, *Proc. R. Soc. A* **392**, 45 (1984).
- [22] F. Wilczek and A. Zee, Linking Numbers, Spin, and Statistics of Solitons, *Phys. Rev. Lett.* **51**, 2250 (1983).
- [23] C. P. Sun and M. L. Ge, Generalizing Born-Oppenheimer approximations and observable effects of an induced gauge field, *Phys. Rev. D* **41**, 1349 (1990).
- [24] J. Ruseckas, G. Juzeliūnas, P. Ohberg, and M. Fleischhauer, Non-Abelian Gauge Potentials for Ultracold Atoms with Degenerate Dark States, *Phys. Rev. Lett.* **95**, 010404 (2005).
- [25] S. L. Zhu, H. Fu, C. J. Wu, S. C. Zhang, and L. M. Duan, Spin Hall Effects for Cold Atoms in a Light-Induced Gauge Potential, *Phys. Rev. Lett.* **97**, 240401 (2006).
- [26] See Supplemental Material at <http://link.aps.org/supplemental/10.1103/PhysRevLett.129.220402> for detailed theoretical proposal and experimental realization.
- [27] Notably, the simplest configuration for instantons should be an array with alternating $n = 0$ and $n = 1$ synthetic vacua, as shown in Fig. S1 in Supplemental Material [26].
- [28] J. E. Moore, Y. Ran, and X. G. Wen, Topological Surface States in Three-Dimensional Magnetic Insulators, *Phys. Rev. Lett.* **101**, 186805 (2008).
- [29] X.-X. Yuan, L. He, S.-T. Wang, D.-L. Deng, F. Wang, W.-Q. Lian, X. Wang, C.-H. Zhang, H.-L. Zhang, X.-Y. Chang, and L.-M. Duan, Observation of Topological Links Associated with Hopf Insulators in a Solid-State Quantum Simulator, *Chin. Phys. Lett.* **34**, 060302 (2017).
- [30] In our experiment, the dependence of the Hamiltonian on position \mathbf{r} is realized by engineering the Raman coupling parameters for a specified position. Thus, we are free to choose the length scale as the unit of position \mathbf{r} . For the sake of simplicity, η is taken to equal 1.
- [31] The same results are reached when viewing spin textures in the vertical yz plane with $x = 0$. Although there are several points where the measured spin textures show large errors limited by the finite fidelity of Hamiltonian preparation, the experimentally measured spin textures clearly reveal the topology of non-Abelian vacua.
- [32] L. Faddeev and A. J. Niemi, Partially Dual Variables in SU(2) Yang-Mills Theory, *Phys. Rev. Lett.* **82**, 1624 (1999).
- [33] J. S. B. Tai and I. I. Smalyukh, Static Hopf Solitons and Knotted Emergent Fields in Solid-State Noncentrosymmetric Magnetic Nanostructures, *Phys. Rev. Lett.* **121**, 187201 (2018).
- [34] I. Belopolski *et al.*, Observation of a linked-loop quantum state in a topological magnet, *Nature (London)* **604**, 647 (2022).
- [35] M. C. Banuls *et al.*, Simulating lattice gauge theories within quantum technologies, *Eur. Phys. J. D* **74**, 165 (2020).